


Superconductivity, pseudogap, and phase separation in topological flat bandsJohannes S. Hofmann ¹, Erez Berg ^{1,*} and Debanjan Chowdhury ^{2,†}¹*Department of Condensed Matter Physics, Weizmann Institute of Science, Rehovot 76100, Israel*²*Department of Physics, Cornell University, Ithaca, New York 14853, USA* (Received 20 January 2020; revised 13 May 2020; accepted 19 October 2020; published 11 November 2020)

Superconductivity is a macroscopic quantum phenomenon that requires electron pairs to delocalize over large distances. A long-standing question is whether superconductivity can exist even if the electrons' kinetic energy is completely quenched, as is the case in a flat band. This is fundamentally a nonperturbative problem, since the interaction energy scale is the only relevant energy scale, and hence it requires going beyond the traditional Bardeen-Cooper-Schrieffer theory of superconductivity, which is perturbative by nature. In this work, we study a two-dimensional model of an isolated narrow band at partial filling with local attractive interactions, using numerically exact quantum Monte Carlo calculations. We focus on the case where the flat bands are *topologically nontrivial*, and hence the single-particle wave functions that span these bands cannot be completely spatially localized. Our calculations unambiguously demonstrate that the ground state is a superconductor; strikingly, the critical temperature scales nearly linearly with the interaction strength. Above the superconducting transition temperature, we find a broad pseudogap regime that exhibits strong pairing fluctuations and a tendency towards electronic phase separation. Introducing a small nearest-neighbor attraction suppresses superconductivity entirely and drives the system to phase separate. We discuss the possible relevance of superconductivity in this unusual regime to the physics of flat band moiré materials.

DOI: [10.1103/PhysRevB.102.201112](https://doi.org/10.1103/PhysRevB.102.201112)

Introduction. What is the highest attainable superconducting temperature T_c in a given system? This decades-old question has become pressing with the discovery of superconductivity in two-dimensional materials with moiré superlattices [1–5], which offer unprecedented control over the electronic band structure and density. It is natural to ask what sets T_c in these systems, as a step towards optimizing it further. In general, T_c is limited by two different energy scales: the pairing scale associated with Cooper pair formation, and the phase ordering (or phase coherence) scale, set by the superconducting phase stiffness [6]. Optimizing one energy scale often comes at the expense of the other. For example, in the paradigmatic attractive Hubbard model, increasing the interaction strength beyond a certain limit decreases the phase ordering temperature; the optimal T_c is achieved when the attractive interaction U and the electronic bandwidth W are comparable, and the maximum attainable T_c is about $0.02W$ [7,8].

Intriguingly, it has been suggested that in certain cases, superconductivity can survive even in the limit where the active electronic bands become perfectly flat [9–13]. As long as the interaction strength is much smaller than the gap between the active narrow band and the other bands, one expects T_c to be proportional to U , which is effectively the only energy scale in the problem. The phase stiffness need not vanish even as the bandwidth vanishes, as long as the single-particle states cannot all be tightly localized [14,15], as in, e.g., topological bands. Note that in this case, upon projecting the problem to the active flat bands, the recently proven upper bound on the

phase stiffness [16] in terms of the bandwidth of the isolated band does not apply, unless contributions from the remote bands are also included [17]. Interestingly, in several moiré systems where superconductivity is found, the active bands have been argued to have a topological character [18–24].

Within Bardeen-Cooper-Schrieffer (BCS) mean-field theory, lower bounds on the phase stiffness in a topological band have been proven [25–28]; however, in the limit of a flat band, the problem is inherently strongly coupled and BCS mean-field theory is generally uncontrolled [29]. In particular, all sorts of competing electronic orders may arise (such as charge order and electronic phase separation), and suppress the superconducting T_c . While studies of superconductivity in flat bands have been performed [25,30–33], superconductivity with $T_c \propto U$ has never been rigorously demonstrated in a solvable model. In addition, the nature of the normal (non-superconducting) state out of which such a superconductor may arise has not been clarified.

In order to address these fundamental questions, we study a sign-problem free lattice electronic model [Fig. 1(a)] with partially filled, flat bands [Fig. 1(b)] with Chern numbers $C = \pm 1$ in the regime of strong attractive interactions using the numerically exact, unbiased determinant quantum Monte Carlo method [34,35]. It has recently been pointed out that the isolated flat bands in magic-angle twisted bilayer graphene can be decomposed into a total of four $C = 1$ and four $C = -1$ bands [36]. Moreover, in a particular solvable limit [37], these Chern bands are tied to a particular sublattice polarization. While the model we study here hosts only two flat $C = \pm 1$ bands and does not directly describe the low-energy physics of any particular material, our study serves as a proof-of-principle for addressing many of the questions raised above,

*erez.berg@weizmann.ac.il

†debanjanchowdhury@cornell.edu

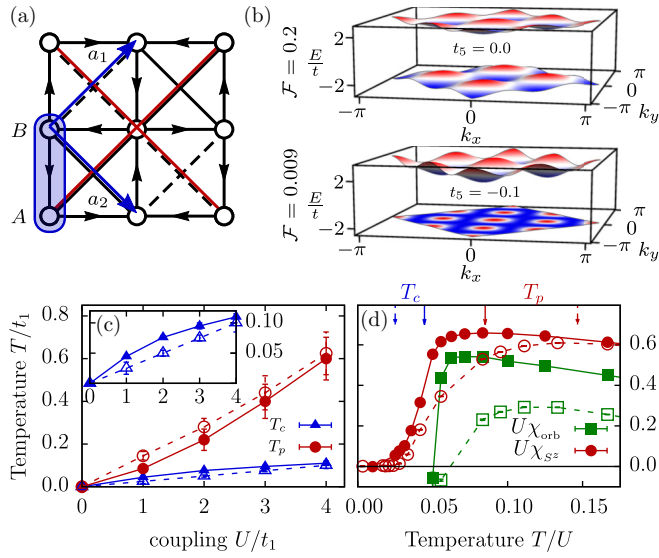


FIG. 1. (a) Lattice model with π flux through every plaquette, two orbitals (A and B), and first, second, and fifth nearest-neighbor hopping of amplitude t_1 , t_2 , and t_5 . (b) Top (bottom): band dispersions for $t_5 = 0.0$ (-0.1) with “flatness ratios” $\mathcal{F} = 0.2$ (0.009). The lower bands have Chern numbers $C = +1$ (-1) for spin-up (spin-down) particles. Red (blue) indicates high (low) energy. (c) The superconducting T_c (in blue) and the “pseudogap temperature,” T_p [in red, defined through the maximum in the spin susceptibility; see panel (d)] as a function of U . Solid and dashed lines correspond to the band structures shown in (b), with $\mathcal{F} = 0.2$ and 0.009 , respectively. (d) The orbital and spin magnetic susceptibilities for the dispersive (flat) band with $U = 1$ ($U = 3$).

paving the way for constructing more realistic models for future studies.

We summarize our main findings as follows: (i) For purely on-site interactions, the ground state is an s -wave superconductor, and in the limit where the electronic bandwidth W is much smaller than U , there is a broad regime of parameters where $T_c \propto U$ [Fig. 1(c)]. (ii) Above T_c , a broad “pseudogap” regime is found, characterized by the opening of a spin gap [Figs. 1(c) and 1(d)] and a gap to single-electron excitations (Fig. 3) without long-range superconductivity. This regime is characterized by two competing tendencies towards superconductivity and towards electronic phase separation (the latter is signaled by an enhanced electronic compressibility), as a consequence of an approximate emergent $SU(2)$ symmetry at low energies [32]. (iii) Adding a small nearest-neighbor attraction breaks the $SU(2)$ symmetry and drives an instability to phase separation, thereby destroying superconductivity (SC).

Model. We consider the Hamiltonian $H = H_{\text{kin}} + H_{\text{int}}$, defined on a two-dimensional (2D) square lattice:

$$H_{\text{kin}} = \left[-t_1 \sum_{\langle i,j \rangle, \sigma} e^{i\phi_{ij}^\sigma} c_{i,\sigma}^\dagger c_{j,\sigma} - t_2 \sum_{\langle i,j \rangle_2, \sigma} s_{(i,j)_2} c_{i,\sigma}^\dagger c_{j,\sigma} - t_5 \sum_{\langle i,j \rangle_5, \sigma} c_{i,\sigma}^\dagger c_{j,\sigma} + \text{H.c.} \right] - \mu \sum_i n_i, \quad (1)$$

$$H_{\text{int}} = -\frac{U}{2} \sum_i (n_i - 1)^2. \quad (2)$$

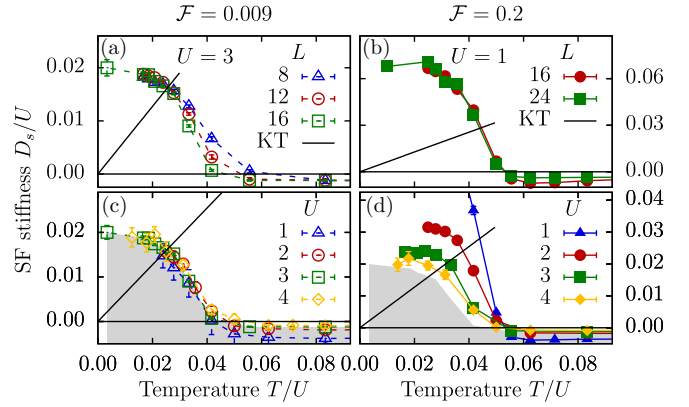


FIG. 2. The superfluid stiffness $D_s(T)$ [Eq. (4)] for the (a) flat-band ($\mathcal{F} = 0.009$, $U = 3$) and (b) dispersive ($\mathcal{F} = 0.2$, $U = 1$) cases, and different system sizes. The black line denotes the universal BKT jump, $D_s = 2T/\pi$. (c) and (d) $D_s(T)$ for various coupling strength U on the largest simulated lattice. In (c), $D_s(T)/U$ curves for different U 's collapse onto each other when plotted vs T/U , confirming that U is effectively the only energy scale in the flat-band case. The shaded area marks the collapsed function in both (c) and (d) to guide the eye for comparison.

Here, $c_{i,\sigma}^\dagger$ ($c_{i,\sigma}$) are fermion creation (annihilation) operators, $n_i = \sum_\sigma c_{i,\sigma}^\dagger c_{i,\sigma}$ is the local density, and t_1 , t_2 , and t_5 denote the first, second, and fifth nearest-neighbor hopping parameters [see Fig. 1(a)], respectively. The single-particle Hamiltonian is a generalization of the model introduced in Ref. [38], designed to give flat bands with Chern numbers $C = \pm 1$. The arrows along the t_1 bonds in Fig. 1(a) mark the direction associated with $\phi_{ij}^\dagger = +\pi/4$, and the solid (dashed) second-neighbor bonds (whose strength is t_2) have a positive (negative) sign $s_{(i,j)_2}$. The red bonds denote t_5 . The density can be tuned by the chemical potential, μ . The phases satisfy $\phi_{ij}^\sigma = -\phi_{ij}^{-\sigma}$, such that time-reversal symmetry is preserved

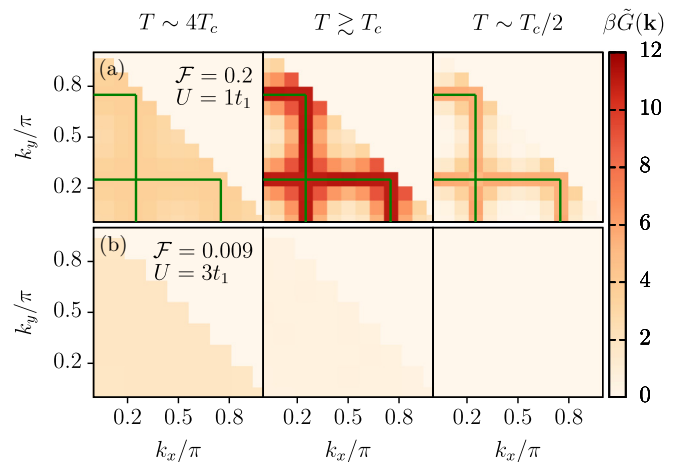


FIG. 3. The quantity $\beta \tilde{G}(\mathbf{k})$, that serves as a proxy for the spectral function near the Fermi energy [see Eq. (5) and the following discussion], as a function of \mathbf{k} . The green lines denote the Fermi surface in the noninteracting case. In (a), $U = 1$ and the temperatures are $T = 0.25, 0.06, 0.03$; in (b), $U = 3$ and $T = 0.4, 0.1, 0.05$.

and $\phi_{ij}^\dagger = \pm \frac{\pi}{4}$ such that each plaquette encloses π flux. $U > 0$ is the strength of a local attractive interaction.

It is convenient to define the vectors $\mathbf{a}_1 \equiv (1, 1)$ and $\mathbf{a}_2 \equiv (1, -1)$; \mathbf{k} then denotes momenta in the Brillouin zone dual to the lattice spanned by $\mathbf{a}_1, \mathbf{a}_2$ [see Fig. 1(a)]. H_{kin} can be written as

$$H_{\text{kin}} = \sum_{\mathbf{k}} \Psi_{\mathbf{k}}^\dagger \hat{H}_{\mathbf{k}} \Psi_{\mathbf{k}}, \quad \hat{H}_{\mathbf{k}} = B_{0,\mathbf{k}} \mathbf{1} + \mathbf{B}_{\mathbf{k}} \cdot \boldsymbol{\tau}, \quad (3)$$

where $\Psi_{\mathbf{k}}^\dagger = (c_{\mathbf{k},A}^\dagger, c_{\mathbf{k},B}^\dagger)$ and $\boldsymbol{\tau} \equiv (\tau_x, \tau_y, \tau_z)$ are the Pauli matrices that act on the sublattice index (A, B).

This leads to two bands, $\varepsilon_{\mathbf{k}} = B_{0,\mathbf{k}} \pm |\mathbf{B}_{\mathbf{k}}|$ [39]. For the remainder of this study, we fix our hopping parameters $t_1 = 1$, $t_2 = 1/\sqrt{2}$ and measure all quantities in units of t_1 . For $t_5 = 0$, the gap between the two bands is $\Delta_{\text{gap}} = 4$ and the bandwidth of the lower band is $W = 0.828$ [Fig. 1(b)]; the ‘‘flatness ratio,’’ $\mathcal{F} \equiv W/\Delta_{\text{gap}} = 0.2$. We can tune the bandwidth of the lower Chern band by varying t_5 . The flatness ratio is minimized by $t_5 = \frac{1-\sqrt{2}}{4}$ where the bandwidth for the lower band, $W \approx 0.035$, while the gap remains at $\Delta_{\text{gap}} = 4$, such that $\mathcal{F} = 0.009$. For most of our study, we focus on (a) $\mathcal{F} = 0.2$ and (b) $\mathcal{F} = 0.009$ for a range of values between $U = 1-4$, and the case of quarter-filling ($\nu = 1/4$), corresponding to a half-filled (lower) Chern band.

Superconductivity. In order to diagnose the possible onset of SC, we compute the phase stiffness D_s . We evaluate the paramagnetic current-current correlation function, $\Lambda_{xx}(\mathbf{q}, i\omega_m = 0)$, at zero external Matsubara frequency and use the relation [7,40]

$$D_s = \frac{1}{4}[-K_x - \Lambda_{xx}(\mathbf{q} = 0)]. \quad (4)$$

Here, $K_x = \langle [\partial^2 H / \partial A_x^2]_{A_x=0} \rangle$ is the diamagnetic current contribution, where A_x is a vector potential in the x direction, introduced via minimal coupling. The $1/4$ prefactor is due to charge-2 Cooper pairs [39]. We plot $D_s(T)$ as a function of temperature in Figs. 2(a) and 2(b). The chemical potential $\mu(T)$ is tuned such that $\nu = 1/4$. In 2D, T_c can be determined from the Berezinskii-Kosterlitz-Thouless (BKT) condition $T_c = \pi D_s^- / 2$, where $D_s^- \equiv D_s(T \rightarrow T_c^-)$. The black solid line denotes the curve $D_s = 2T/\pi$, the intersection of which with $D_s(T)$ gives T_c . The T_c values extracted from $D_s(T)$ are consistent with an independent analysis of the superconducting correlation length ξ_{SC}/L presented in the Supplemental Material [39] (see, also, Ref. [1] therein).

The slightly negative D_s values found at high temperatures are associated with Trotter errors, and we have checked that they decrease in magnitude towards zero upon decreasing the imaginary time step $\Delta\tau$. We have also confirmed the absence of a few possible competing orders such as a charge density wave, a bond density wave, or magnetic states [39].

The BKT transition temperature as a function of U is shown in the inset of Fig. 1(c) for the two band structures with $\mathcal{F} = 0.2, 0.009$. Most strikingly, for the narrower band, T_c depends almost perfectly linearly on U : $T_c \approx 0.025U$. In the case of the more dispersive band, T_c is higher than for the narrower band, and has a downward curvature. As U increases, the T_c 's of the two band structures approach each other. This behavior can be understood in terms of two contributions to the phase stiffness: (i) a geometric contribution originating

from the finite extent of the wave functions spanning the topological bands, that does not vanish even in the $W \rightarrow 0$ limit, and (ii) the conventional contribution originating from the single-particle kinetic energy.

The dependence of T_c on U is hence markedly different both from the conventional weak-coupling BCS behavior, $T_c \sim W e^{-W/U}$, and from the strong-coupling behavior found in the attractive Hubbard model, $T_c \sim W^2/U$. To shed more light into the origin of this behavior, we present in Figs. 2(c) and 2(d) scaling plots of D_s/U as a function of T/U for different values of U . For the narrower band [panel (c)], the curves collapse. This can be understood by considering the limit $W \ll T \ll \Delta_{\text{gap}}$. Since the upper band can effectively be projected out in this regime, the superfluid density must be of the form $D_s = U f(T/U, \nu)$, where f is a scaling function that depends only on the Bloch wave functions of the lower band. Fixing ν gives a scaling collapse of the form observed in Fig. 2(c). For the more dispersive case [panel (d)] the curves do not collapse. As U increases, however, the $\mathcal{F} = 0.2$ curves converge towards the shaded form, which is the scaling function for $\mathcal{F} = 0.009$.

Normal-state properties. Let us now examine the properties of the normal (nonsuperconducting) state for $T > T_c$. In the limit where the bare band is very narrow, the key question is whether the normal state should be understood in terms of coherent quasiparticle excitations whose bandwidth is set by the interaction strength, or as an incoherent liquid of Cooper pairs [41,42]. As described below, our findings are consistent with the latter scenario: as \mathcal{F} decreases, a broad ‘‘pseudogap’’ regime appears above T_c , characterized by the opening of a gap for spin and single-particle excitations. The pseudogap regime further displays strong superconducting fluctuations and a tendency towards phase separation.

In order to probe the single-electron spectral function, $A(\mathbf{k}, \omega) = -\pi^{-1} \text{Im} G(\mathbf{k}, \omega)$, we recall that the imaginary-time Green's function, $G(\mathbf{k}, \tau) = \sum_{\alpha=A,B} \langle c_{\alpha\mathbf{k}}(\tau) c_{\alpha\mathbf{k}}^\dagger(0) \rangle$, for $0 < \tau < \beta$ has the following property [43]:

$$G(\mathbf{k}, \tau) = \int_{-\infty}^{\infty} d\omega \frac{e^{-\omega(\tau-\beta/2)}}{2 \cosh(\beta\omega/2)} A(\mathbf{k}, \omega). \quad (5)$$

Thus, $\tilde{G}(\mathbf{k}) \equiv G(\mathbf{k}, \tau = \beta/2)$ is the integrated spectral weight around the Fermi level over a width of $\sim T$. In particular, $\lim_{T \rightarrow 0} \beta \tilde{G}(\mathbf{k}) = \pi A(\mathbf{k}, \omega = 0)$. Figures 3(a) and 3(b) show the evolution of $\tilde{G}(\mathbf{k})$ as a function of decreasing temperature from $T \sim 4T_c$ down to $T \sim T_c/2$ for two parameter sets, $(\mathcal{F}, U) = (0.2, 1)$ and $(0.009, 3)$.

For the more dispersive band [Fig. 3(a)], $\tilde{G}(\mathbf{k})$ is peaked near the noninteracting Fermi surface (but is significantly broadened). Moreover, even in the SC state at $T \sim T_c/2$, when the Fermi surface develops a SC gap, the remnant of the gapped Bogoliubov spectrum continues to remain visible near the original Fermi surface. On the other hand, for the flatter band at stronger coupling, $\tilde{G}(\mathbf{k})$ is completely featureless across T_c , showing no sign of coherently propagating quasiparticles nor a well-defined Fermi surface. Hence, superconductivity here cannot be understood as a Fermi surface instability.

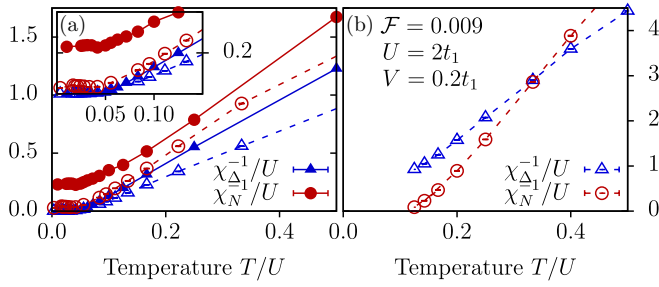


FIG. 4. (a) The reciprocal pairing and charge susceptibilities are shown for $\mathcal{F} = 0.2$, $U = 1t_1$ (solid) and $\mathcal{F} = 0.009$, $U = 3t_1$ (dashed). (b) Same as (a) but with an additional nearest-neighbor interaction $H_{\text{int,nn}}$ [see Eq. (8)], with $V = 0.2t_1$.

The normal state is further characterized by its charge, magnetic (Zeeman and orbital), and pairing susceptibilities, defined as

$$\chi_{\Delta} = L^{-2} \int_0^{\beta} d\tau \langle \hat{O}(\tau) \hat{O}(\tau = 0) \rangle, \quad (6)$$

$$\chi_{\text{orb}} = \lim_{q \rightarrow 0} q^{-2} [\Lambda_{xx}^t(q) - \Lambda_{xx}^l(q)], \quad (7)$$

with \hat{O} being the total z component of the spin ($S^z = \sum_j c_j^\dagger \sigma^z c_j$), charge [$N = \sum_j (n_j - \nu)$], and s -wave pairing ($\Delta = \sum_j c_{j,\uparrow} c_{j,\downarrow} + \text{H.c.}$), respectively. For the orbital magnetic susceptibility, we use the notation $\Lambda_{xx}^t(q) = \Lambda_{xx}(q_x = 0, q_y = q)$ and $\Lambda_{xx}^l(q) = \Lambda_{xx}(q_x = q, q_y = 0)$ for the transverse and longitudinal components [39].

The spin and orbital magnetic susceptibilities are presented in Fig. 1(d). The spin susceptibility, χ_{S^z} , shows a clear suppression below a characteristic temperature scale, indicating the onset of a spin gap. We define the ‘‘pseudogap temperature’’ T_p as the location of the maximum of $\chi_{S^z}(T)$, shown in Fig. 1(c) as a function of U , and is found to be substantially above T_c at strong coupling. χ_{orb} is positive (paramagnetic) at high temperature, but drops sharply and becomes large and negative (diamagnetic) at a temperature above T_c . The sign change in χ_{orb} occurs at $T \approx 0.05U$ [Fig. 1(d)]. This behavior can be understood as the consequence of the onset of pairing fluctuations, which give a diamagnetic contribution to the orbital susceptibility.

Finally, we present the reciprocal pairing and charge susceptibilities, χ_{Δ}^{-1} , χ_N^{-1} , in Fig. 4(a). For a broad range in temperature below Δ_{gap} and above T_c , the pairing susceptibility appears to follow a Curie-Weiss law $\chi_{\Delta} \sim (T - \Theta)^{-1}$. Strikingly, the charge susceptibility χ_N is also strongly enhanced in the same temperature regime. This signals a tendency towards phase separation, driven by the same attractive interaction that is responsible for superconductivity. Phase separation is ultimately preempted by superconductivity, and χ_N saturates below T_c . The enhancement of χ_N with decreasing temperature is particularly strong for the narrower band. This can be understood as a consequence of an emergent SU(2) symmetry in the limit $\mathcal{F} \rightarrow 0$ and $U/\Delta_{\text{gap}} \rightarrow 0$ [32,39]. Here, the BCS wave function is an exact ground state. The SU(2) symmetry relates the superconducting susceptibility to the charge susceptibility; hence, $\chi_{\Delta} = \chi_N$, and both diverge in the limit $T \rightarrow 0$.

In our system, the SU(2) symmetry is weakly broken, due to both the finite U/Δ_{gap} and the nonzero bandwidth [39]. This tilts the balance in favor of superconductivity, rendering T_c finite and saturating χ_N . Interestingly, in the case of the more dispersive band, χ_N continues to be temperature dependent even for $T < W = 0.828t_1$. This is reminiscent of the behavior observed in the repulsive Hubbard model at intermediate temperatures [44,45].

The close competition between superconductivity and phase separation suggests that the superconducting state is fragile. To demonstrate this, we studied the effect of adding nearest-neighbor interactions to our original Hamiltonian,

$$H_{\text{int,nn}} = -V \sum_{\langle i,j \rangle} (n_i - 1)(n_j - 1). \quad (8)$$

Figure 4(b) shows $\chi_{\Delta}^{-1}(T)$, $\chi_N^{-1}(T)$ for $V = 0.1U = 0.2t_1$. The nearest-neighbor interaction drives a finite-temperature instability towards phase separation, signaled by $\chi_N^{-1} \rightarrow 0$, that preempts the superconducting transition. This fragility of the superconducting state is a consequence of the approximate SU(2) symmetry; the nearest-neighbor attraction breaks the symmetry and favors phase separation. Note that this is a strong-coupling effect, not attainable within a BCS treatment of the problem.

Discussion and outlook. We have demonstrated explicitly that superconductivity is possible in the limit of nearly flat bands in the presence of local attractive interactions. In this strong-coupling regime, the interaction strength is the dominant energy scale; consequently, $T_c \propto U$. Moreover, superconductivity emerges from a pseudogap regime, where single-particle and spin excitations are gapped, and superconducting as well as particle number fluctuations are strongly enhanced. The close competition between the tendencies towards superconductivity and phase separation is a result of an emergent SU(2) symmetry that relates the two. The low-energy physics can be captured by a nonlinear sigma model (NLSM), supplemented by a small anisotropic term that favors either SC or phase separation [39].

Clearly, an essential ingredient for superconductivity in the flat-band regime is the geometric character of the band; it is crucial that the wave functions spanning the band are not completely localizable [25,26]. The minimal spatial extent of the wave functions, set by the ‘‘quantum metric’’ of the band [15], ultimately determines the kinetic energy of the Cooper pairs. An interesting open question, worthy of further investigations, is to what extent is band topology essential for superconductivity in this regime.

Finally, we speculate about the relevance of the physics discussed here to superconductivity in two-dimensional moiré materials. In these systems, superconductivity is indeed found in extremely narrow, topologically nontrivial bands. It would be interesting to look for a pseudogap regime above the superconducting T_c , characterized by strong pairing fluctuations and an enhanced electronic compressibility. Incidentally, indirect signatures of a possible pseudogap above T_c have been reported in twisted bilayer graphene [46].

Acknowledgments. The authors thank F. Assaad, F. P. Toldin, T. Holder, and M. Randeria for stimulating discussions. D.C. is supported by faculty startup funds at Cornell

University. D.C. also acknowledges the hospitality of the Weizmann Institute of Science and the Max-Planck Institute for the Physics of Complex Systems. E.B. and J.H. were supported by the European Research Council (ERC) under grant HQMAT (Grant No. 817799), and by the US–Israel Binational Science Foundation (BSF). The authors grate-

fully acknowledge the Gauss Centre for Supercomputing e.V. [48] for funding this project by providing computing time on the GCS Supercomputer SuperMUC at Leibniz Supercomputing Centre [49] under Project No. pr53ju. This work was supported by a research grant from Irving and Cherna Moskowitz.

-
- [1] Y. Cao, V. Fatemi, S. Fang, K. Watanabe, T. Taniguchi, E. Kaxiras, and P. Jarillo-Herrero, Unconventional superconductivity in magic-angle graphene superlattices, *Nature (London)* **556**, 43 (2018).
- [2] M. Yankowitz, S. Chen, H. Polshyn, Y. Zhang, K. Watanabe, T. Taniguchi, D. Graf, A. F. Young, and C. R. Dean, Tuning superconductivity in twisted bilayer graphene, *Science* **363**, 1059 (2019).
- [3] X. Lu, P. Stepanov, W. Yang, M. Xie, M. A. Aamir, I. Das, C. Urgell, K. Watanabe, T. Taniguchi, G. Zhang, A. Bachtold, A. H. MacDonald, and D. K. Efetov, Superconductors, orbital magnets and correlated states in magic-angle bilayer graphene, *Nature (London)* **574**, 653 (2019).
- [4] G. Chen, A. L. Sharpe, P. Gallagher, I. T. Rosen, E. J. Fox, L. Jiang, B. Lyu, H. Li, K. Watanabe, T. Taniguchi, J. Jung, Z. Shi, D. Goldhaber-Gordon, Y. Zhang, and F. Wang, Signatures of tunable superconductivity in a trilayer graphene moiré superlattice, *Nature (London)* **572**, 215 (2019).
- [5] X. Liu, Z. Hao, E. Khalaf, J. Y. Lee, K. Watanabe, T. Taniguchi, A. Vishwanath, and P. Kim, Spin-polarized correlated insulator and superconductor in twisted double bilayer graphene, *Nature (London)* **583**, 221 (2020).
- [6] V. Emery and S. Kivelson, Importance of phase fluctuations in superconductors with small superfluid density, *Nature (London)* **374**, 434 (1995).
- [7] T. Paiva, R. R. dos Santos, R. T. Scalettar, and P. J. H. Denteneer, Critical temperature for the two-dimensional attractive Hubbard model, *Phys. Rev. B* **69**, 184501 (2004).
- [8] T. Paiva, R. Scalettar, M. Randeria, and N. Trivedi, Fermions in 2D Optical Lattices: Temperature and Entropy Scales for Observing Antiferromagnetism and Superfluidity, *Phys. Rev. Lett.* **104**, 066406 (2010).
- [9] V. Shaginyan and V. Khodel, Superfluidity in system with fermion condensate, *JETP Lett.* **51**, 553 (1990).
- [10] T. T. Heikkilä, N. B. Kopnin, and G. E. Volovik, Flat bands in topological media, *JETP Lett.* **94**, 233 (2011).
- [11] N. B. Kopnin, T. T. Heikkilä, and G. E. Volovik, High-temperature surface superconductivity in topological flat-band systems, *Phys. Rev. B* **83**, 220503(R) (2011).
- [12] N. B. Kopnin, Surface superconductivity in multilayered rhombohedral graphene: Supercurrent, *JETP Lett.* **94**, 81 (2011).
- [13] G. E. Volovik, Flat band in topological matter, *J. Supercond. Novel Magn.* **26**, 2887 (2013).
- [14] N. Marzari and D. Vanderbilt, Maximally localized generalized Wannier functions for composite energy bands, *Phys. Rev. B* **56**, 12847 (1997).
- [15] N. Marzari, A. A. Mostofi, J. R. Yates, I. Souza, and D. Vanderbilt, “Maximally localized Wannier functions: Theory and applications,” *Rev. Mod. Phys.* **84**, 1419 (2012).
- [16] T. Hazra, N. Verma, and M. Randeria, Bounds on the Superconducting Transition Temperature: Applications to Twisted Bilayer Graphene and Cold Atoms, *Phys. Rev. X* **9**, 031049 (2019).
- [17] The interaction term, when projected to the isolated topological bands, becomes nontrivial and contributes to the electron current. The stiffness can then no longer be bounded by the kinetic energy terms alone.
- [18] H. C. Po, L. Zou, A. Vishwanath, and T. Senthil, Origin of Mott Insulating Behavior and Superconductivity in Twisted Bilayer Graphene, *Phys. Rev. X* **8**, 031089 (2018).
- [19] L. Zou, H. C. Po, A. Vishwanath, and T. Senthil, Band structure of twisted bilayer graphene: Emergent symmetries, commensurate approximants, and Wannier obstructions, *Phys. Rev. B* **98**, 085435 (2018).
- [20] H. C. Po, L. Zou, T. Senthil, and A. Vishwanath, Faithful tight-binding models and fragile topology of magic-angle bilayer graphene, *Phys. Rev. B* **99**, 195455 (2019).
- [21] Z. Song, Z. Wang, W. Shi, G. Li, C. Fang, and B. A. Bernevig, All Magic Angles in Twisted Bilayer Graphene are Topological, *Phys. Rev. Lett.* **123**, 036401 (2019).
- [22] J. Ahn, S. Park, and B.-J. Yang, Failure of Nielsen-Ninomiya Theorem and Fragile Topology in Two-Dimensional Systems with Space-Time Inversion Symmetry: Application to Twisted Bilayer Graphene at Magic Angle, *Phys. Rev. X* **9**, 021013 (2019).
- [23] G. Chen, L. Jiang, S. Wu, B. Lyu, H. Li, B. L. Chittari, K. Watanabe, T. Taniguchi, Z. Shi, J. Jung, Y. Zhang, and F. Wang, Evidence of a gate-tunable Mott insulator in a trilayer graphene moiré superlattice, *Nat. Phys.* **15**, 237 (2019).
- [24] G. Chen, A. L. Sharpe, E. J. Fox, Y.-H. Zhang, S. Wang, L. Jiang, B. Lyu, H. Li, K. Watanabe, T. Taniguchi, Z. Shi, T. Senthil, D. Goldhaber-Gordon, Y. Zhang, and F. Wang, Tunable correlated Chern insulator and ferromagnetism in a moiré superlattice, *Nature* **579**, 56 (2020).
- [25] S. Peotta and P. Törmä, Superfluidity in topologically nontrivial flat bands, *Nat. Commun.* **6**, 8944 (2015).
- [26] F. Xie, Z. Song, B. Lian, and B. A. Bernevig, Topology-Bounded Superfluid Weight in Twisted Bilayer Graphene, *Phys. Rev. Lett.* **124**, 167002 (2020).
- [27] A. Julku, T. J. Peltonen, L. Liang, T. T. Heikkilä, and P. Törmä, Superfluid weight and Berezinskii-Kosterlitz-Thouless transition temperature of twisted bilayer graphene, *Phys. Rev. B* **101**, 060505(R) (2020).
- [28] X. Hu, T. Hyart, D. I. Pikulin, and E. Rossi, Geometric and Conventional Contribution to Superfluid Weight in Twisted Bilayer Graphene, *Phys. Rev. Lett.* **123**, 237002 (2019).
- [29] If the active band is precisely flat and particle-hole symmetric, then the BCS wave function is exact [25], due to an SU(2) symmetry that relates the charge and pairing operators. Under

- these conditions, $T_c = 0$. An approximate SU(2) symmetry may also emerge at low energies under certain conditions [32], as we discuss in detail below.
- [30] V. I. Iglovikov, F. Hébert, B. Grémaud, G. G. Batrouni, and R. T. Scalettar, Superconducting transitions in flat-band systems, *Phys. Rev. B* **90**, 094506 (2014).
- [31] A. Julku, S. Peotta, T. I. Vanhala, D.-H. Kim, and P. Törmä, Geometric Origin of Superfluidity in the Lieb-lattice Flat Band, *Phys. Rev. Lett.* **117**, 045303 (2016).
- [32] M. Tovmasyan, S. Peotta, P. Törmä, and S. D. Huber, Effective theory and emergent SU(2) symmetry in the flat bands of attractive Hubbard models, *Phys. Rev. B* **94**, 245149 (2016).
- [33] L. Liang, T. I. Vanhala, S. Peotta, T. Siro, A. Harju, and P. Törmä, Band geometry, Berry curvature, and superfluid weight, *Phys. Rev. B* **95**, 024515 (2017).
- [34] R. Blankenbecler, D. J. Scalapino, and R. L. Sugar, Monte Carlo calculations of coupled boson-fermion systems, *Phys. Rev. D* **24**, 2278 (1981).
- [35] M. Bercx, F. Goth, J. S. Hofmann, and F. F. Assaad, The ALF (Algorithms for Lattice Fermions) project release 1.0. Documentation for the auxiliary field quantum Monte Carlo code, *SciPost Phys.* **3**, 013 (2017).
- [36] N. Bultinck, E. Khalaf, S. Liu, S. Chatterjee, A. Vishwanath, and M. P. Zaletel, Ground State and Hidden Symmetry of Magic Angle Graphene at Even Integer Filling, *Phys. Rev. X* **10**, 031034 (2020).
- [37] G. Tarnopolsky, A. J. Kruchkov, and A. Vishwanath, Origin of Magic Angles in Twisted Bilayer Graphene, *Phys. Rev. Lett.* **122**, 106405 (2019).
- [38] T. Neupert, L. Santos, C. Chamon, and C. Mudry, Fractional Quantum Hall States at Zero Magnetic Field, *Phys. Rev. Lett.* **106**, 236804 (2011).
- [39] See Supplemental Material at <http://link.aps.org/supplemental/10.1103/PhysRevB.102.201112> for more details on the explicit form of \mathbf{B}_k , the current operator, phase stiffness, analysis of T_c through the SC correlation length, the density of states near the Fermi level, the dependence of T_c on filling, competing orders, the momentum dependence of $\Lambda_{xx}^1(q) - \Lambda_{xx}^2(q)$, and the approximate low-energy SU(2) symmetry and corresponding NLSM description. This includes Ref. [47].
- [40] D. J. Scalapino, S. R. White, and S. Zhang, Insulator, metal, or superconductor: The criteria, *Phys. Rev. B* **47**, 7995 (1993).
- [41] M. Tovmasyan, S. Peotta, L. Liang, P. Törmä, and S. D. Huber, Preformed pairs in flat Bloch bands, *Phys. Rev. B* **98**, 134513 (2018).
- [42] For a recent discussion of pseudogaps in two-dimensional superconductors, see X. Wang, C. Qijin and K. Levin, Strong pairing in two dimensions: Pseudogaps, domes, and other implications, *New J. Phys.* **22**, 063050 (2020).
- [43] N. Trivedi and M. Randeria, Deviations from Fermi-Liquid Behavior Above T_c in 2D Short Coherence Length Superconductors, *Phys. Rev. Lett.* **75**, 312 (1995).
- [44] P. T. Brown, D. Mitra, E. Guardado-Sanchez, R. Nourafkan, A. Reymbaut, C.-D. Hébert, S. Bergeron, A.-M. S. Tremblay, J. Kokalj, D. A. Huse, P. Schauß, and W. S. Bakr, Bad metallic transport in a cold atom Fermi-Hubbard system, *Science* **363**, 379 (2019).
- [45] E. W. Huang, R. Sheppard, B. Moritz, and T. P. Devereaux, Strange metallicity in the doped Hubbard model, *Science* **366**, 987 (2019).
- [46] Y. Cao, D. Chowdhury, D. Rodan-Legrain, O. Rubies-Bigordà, K. Watanabe, T. Taniguchi, T. Senthil, and P. Jarillo-Herrero, Strange Metal in Magic-Angle Graphene with Near Planckian Dissipation, *Phys. Rev. Lett.* **124**, 076801 (2020).
- [47] F. Parisen Toldin, M. Hohenadler, F. F. Assaad, and I. F. Herbut, Fermionic quantum criticality in honeycomb and π -flux Hubbard models: Finite-size scaling of renormalization-group-invariant observables from quantum Monte Carlo, *Phys. Rev. B* **91**, 165108 (2015).
- [48] www.gauss-centre.eu.
- [49] www.lrz.de.